INSTITUTE OF PHYSICS PUBLISHING JOURNAL OF PHYSICS B: ATOMIC, MOLECULAR AND OPTICAL PHYSICS

J. Phys. B: At. Mol. Opt. Phys. **34** (2001) 3179–3191 PII: S0953-4075(01)24246-1

A radiation-damped R-matrix approach to the electron-impact excitation of helium-like ions for diagnostic application to fusion and astrophysical plasmas

A D Whiteford, N R Badnell, C P Ballance, M G O'Mullane, H P Summers and A L Thomas

Department of Physics and Applied Physics, University of Strathclyde, Glasgow G4 0NG, UK

Received 19 April 2001, in final form 12 June 2001
Published 23 July 2001
Online at stacks.iop.org/JPhysB/34/3179

Abstract

Electron-impact excitation collision strengths for transitions between all singly excited levels up to the $n = 4$ shell of helium-like argon and the $n = 4$ and 5 shells of helium-like iron have been calculated using a radiation-damped R-matrix approach. The theoretical collision strengths have been examined and associated with their infinite-energy limit values to allow the preparation of Maxwell-averaged effective collision strengths. These are conservatively considered to be accurate to within 20% at all temperatures, 3×10^5–3×10^8 K for Ar^{16+} and 10^6–10^9 K for Fe^{24+}. They have been compared with the results of previous studies, where possible, and we find a broad accord.

The corresponding rate coefficients are required for use in the calculation of derived, collisional–radiative, effective emission coefficients for helium-like lines for diagnostic application to fusion and astrophysical plasmas. The uncertainties in the fundamental collision data have been used to provide a critical assessment of the expected resultant uncertainties in such derived data, including redistributive and cascade collisional–radiative effects. The consequential uncertainties in the parts of the effective emission coefficients driven by excitation from the ground levels for the key w, x, y and z lines vary between 5% and 10%. Our results remove an uncertainty in the reaction rates of a key class of atomic processes governing the spectral emission of helium-like ions in plasmas.

1. Introduction

The spectral emission of highly charged helium-like ions has been used heavily in the diagnostic analysis of solar coronal and laboratory plasmas since the 1960s. Its value stems from the fact that the ionization equilibrium fractional abundance of the helium-like ionization stage has an

extended temperature range. This leads to large spectral intensities in temperature-stratified plasmas such as the chromosphere and corona. Thus, collectively, the helium-like ionization stages of elements span virtually all temperature regimes of a plasma. Hence, a particular zone of a plasma may be studied by the emission lines of the helium-like ion which exists there. In recognition of this, soft x-ray instruments such as the bent crystal spectrometer (BCS) on the *SMM* satellite were targeted on these lines. This practice has continued to the present with satellites such as *YOHKOH* for solar studies and *Chandra* and *XMM–Newton* for deep-space observations. In view of these new high-quality observations, it is timely to re-appraise the atomic data entering the interpretation of helium-like systems. This work also forms part of that of the RmaX Network[1], whose focus is on electron- and photon-induced x-ray transitions.

Cross section calculations are performed to enable the prediction of a number of key line ratios such as the G-ratio and the x/y-ratio, whose importance were first pointed-out by Gabriel (1972). These ratios are influenced by electron-impact excitation and recombination. The focus here is on the precision of the excitation part.

The simple Van Regemorter (1962) P-factor[2] approach to the rate coefficients used by Gabriel (1972) was replaced by the results of distorted-wave calculations for a number of astrophysically important elements by Jones (1974), along with additional distorted-wave work by a number of authors, of which Bhatia and Tempkin (1977) is representative. These calculations were restricted to levels with $n \leqslant 2$. Sampson *et al* (1983) extended them, from $n = 1$ and 2, to all levels up to $n = 5$. All of these calculations ignored resonances.

The effect of resonances was considered by Pradhan (1983a, b). He used multi-channel quantum defect theory (MQDT) and a combined close-coupling and distorted-wave approach to examine the effect on the effective collision strengths of resonances (including damping) converging on the $n = 2$ and 3 thresholds. For Fe^{24+}, he found almost a factor of two resonant enhancement for the forbidden transition $1s^2\ {}^1S_0$–$1s2s\ {}^3S_1$ and $\approx$10% reduction due to damping, both at a temperature of $\sim 10^7$ K. The peak coronal abundance of Fe^{24+} lies at about 3×10^7 K. Effective collision strengths, including resonances and damping, were presented by Pradhan (1985) for 78 transitions between the lowest 13 levels (i.e. up to the $1s3p\ {}^3P_2$ level) of Ca^{18+} and Fe^{24+}.

Zhang and Sampson (1987) have used a distorted-wave method along with a perturbative approach to resonances and their damping. They allowed for resonances converging on the $n = 3$ thresholds only. This should suffice for highly charged ions. They presented effective collision strengths for the 21 transitions between the lowest seven levels (i.e. up to the $1s2p\ {}^1P_1$ level) for 18 ions spanning $Z = 8$–74.

Limited R-matrix calculations have been carried-out for O^{6+} and Mg^{10+} by Tayal and Kingston (1984, 1985). More recently, Kimura *et al* (2000) have carried-out 31-level (i.e. up to $n = 4$) Dirac–Fock R-matrix calculations so as to generate effective collision strengths for three helium-like ions, including Fe^{24+}. Results were obtained only for the 16 transitions from the ground level up to the $n = 2$ and 3 levels. They did not allow for radiation damping. Present computing resources indicate that a state-of-the-art R-matrix calculation is possible for helium-like ions, including radiation damping, extending to all 1176 transitions that arise between singly excited levels up to $n = 5$ in an intermediate coupling picture. We report on such a 49-level R-matrix calculation here for Fe^{24+}, as well as a 31-level calculation (i.e. up to $n = 4$) so as to assess the effect of extrapolation of $n = 4$ data versus $n = 5$ data on key diagnostic line ratios. We report also on an $n = 4$ calculation alone for Ar^{16+}.

[1] http://amdpp.phys.strath.ac.uk/UK_RmaX/

[2] The Maxwell-averaged $\overline{g}$-factor.

Finally, we note that Wong *et al* (1995) have measured electron-impact excitation cross sections for the w, x, y and z lines in Fe^{24+}, just above the $n = 2$ thresholds, using an electron-beam ion-trap. Given the experimental uncertainties and the need to correct for cascades, they found broad accord with the results of several theoretical groups, including those of an R-matrix calculation by Zhang and Pradhan (1995). Only the non-resonant background cross section was measured though. However, Chantrenne *et al* (1992) carried out a similar measurement for the helium-like ion Ti^{20+} but were able to span a wider range of energies above the $n = 2$ thresholds and presented results that included the KMn resonances. These results are in broad accord with the radiation damped R-matrix results of Gorczyca *et al* (1995).

The structure of this paper is as follows. In section 2 we discuss the details of our collision strength calculations and present some results illustrating their high-energy behaviour. In section 3 we make some comparisons of our effective collision strengths with those of other workers; we discuss also the application of our data to collisional–radiative modelling and carry-out an error analysis for selected line ratios. We finish with a short conclusion.

2. Calculations and results

2.1. Methodology

Our approach to the determination of radiation damped collision strengths is to use the R-matrix method (Burke and Berrington 1993) in conjunction with the intermediate coupling frame transformation (ICFT) method (Griffin *et al* 1998) and the optical potential approach to damping (Robicheaux *et al* 1995, Gorczyca and Badnell 1996). A complete solution, in terms of reactance or scattering (collision) matrices is obtained firstly in LS-coupling. In particular, use is made of multi-channel quantum defect theory to obtain 'unphysical' collision matrices (as implemented by Gorczyca and Badnell (2000)). These are then transformed, first, algebraically to jK-coupling and then, via the use of the term-coupling coefficients, to intermediate coupling. The key advantages of using this method versus the equivalent full Breit–Pauli R-matrix approach, and also some of the computational issues, are outlined by Badnell and Griffin (2001). Suffice it to say, at this time, the ICFT method is computationally less demanding than the full Breit–Pauli approach but does not suffer the inaccuracies associated with the term coupling of physical collision matrices. Finally, we note that the use of the optical potential modifies the usual (undamped) expressions for the R-matrix, unphysical collision matrices and MQDT closure relations by making them complex, in general, see Robicheaux *et al* (1995) for details.

2.2. Atomic structure calculation details

We used AUTOSTRUCTURE (Badnell 1997) to calculate the atomic structure and, hence, to generate radial wavefunctions for the collision calculation. Table 1 summarizes the energy-level results in comparison with those of NIST (2001). Agreement is very good (within 0.13% for Ar^{16+} and 0.17% for Fe^{24+}) with the 1s2s $^1S_0$ level being the worst case. It should be noted that we have omitted the two-body fine-structure and non-fine-structure Breit–Pauli operators from our AUTOSTRUCTURE calculations since they are not present in the R-matrix codes. Examples of more precise calculations for the $n = 1$ and 2 shells can be found in Plante *et al* (1994) and also Drake (1988).

For dipole-allowed transitions, the length and velocity forms of the oscillator strengths agreed to within 3% (Ar^{16+}) and 4% (Fe^{24+}) for the $1s^2\ ^1S_0$–$1snp\ ^1P_1$ series, to within 5%

Table 1. Energy levels (cm^{-1}) of Ar^{16+} and Fe^{24+}, up to $n = 4$.

	Ar^{16+}		Fe^{24+}	
Level	Present	NIST[a]	Present	NIST
$1s^2\ ^1S_0$	0	0	0	0
$1s2s\ ^3S_1$	25 061 788	25 036 585	53 608 482	53 527 090
$1s2s\ ^1S_0$	25 227 719	25 200 958	53 858 375	53 781 300
$1s2p\ ^3P_0$	25 207 029	25 187 783	53 822 873	53 760 280
$1s2p\ ^3P_1$	25 216 430	25 192 896	53 853 844	53 779 140
$1s2p\ ^3P_2$	25 240 697	25 215 174	53 976 753	53 895 550
$1s2p\ ^1P_1$	25 354 018	25 322 193	54 129 514	54 040 000
$1s3s\ ^3S_1$	29 661 294	29 633 330	63 507 258	63 421 610
$1s3s\ ^1S_0$	29 703 843	29 676 817	63 570 330	63 488 390
$1s3p\ ^3P_0$	29 701 043	29 674 992	63 565 901	63 486 290
$1s3p\ ^3P_1$	29 703 670	29 676 554	63 574 243	63 490 690
$1s3p\ ^3P_2$	29 710 675	29 683 166	63 609 903	63 525 620
$1s3p\ ^1P_1$	29 740 741	29 712 200	63 649 896	63 565 470
$1s3d\ ^3D_1$	29 733 631	—	63 643 861	—
$1s3d\ ^3D_2$	29 734 111	—	63 644 768	—
$1s3d\ ^3D_3$	29 736 831	—	63 658 602	—
$1s3d\ ^1D_2$	29 737 983	—	63 660 201	—
$1s4s\ ^3S_1$	31 248 528	31 219 900	66 933 257	66 847 000
$1s4s\ ^1S_0$	31 265 381	31 238 100	66 957 978	66 874 060
$1s4p\ ^3P_0$	31 264 789	31 273 331	66 957 245	66 873 940
$1s4p\ ^3P_1$	31 265 847	31 238 000	66 960 570	66 875 780
$1s4p\ ^3P_2$	31 268 713	31 240 787	66 975 228	66 890 550
$1s4p\ ^1P_1$	31 280 856	31 253 100	66 991 257	66 906 790
$1s4d\ ^3D_1$	31 278 006	—	66 988 969	—
$1s4d\ ^3D_2$	31 278 242	—	66 989 436	—
$1s4d\ ^3D_3$	31 279 348	—	66 995 140	—
$1s4d\ ^1D_2$	31 279 983	—	66 996 006	—
$1s4f\ ^3F_2$	31 279 887	—	66 995 877	—
$1s4f\ ^3F_3$	31 279 892	—	66 995 886	—
$1s4f\ ^3F_4$	31 280 560	—	66 998 975	—
$1s4f\ ^1F_3$	31 280 567	—	66 998 986	—

[a] NIST database (http://physics.nist.gov/).

(Ar^{16+}) and 6% (Fe^{24+}) for the $1s2s\ ^3S_1$–$1s3p\ ^3P_{0,1,2}$ transitions and to within 11% (Ar^{16+}) and 14% (Fe^{24+}) for the $1s2s\ ^3S_1$–$1s4p\ ^3P_{0,1,2}$ transitions.

The variation between the length and velocity forms is much larger for the $1s2s\ ^3S_1$–$1s2p\ ^3P_{0,1,2}$ transitions due to the long-range radial overlaps. The length form is to be preferred and this is the relevant form for assessing the accuracy of the resultant collision strengths. In the case of Fe^{24+}, the present A-values for these transitions agreed with those of NIST (2001) to within 4%, 27% and 14% for $J = 0, 1, 2$, respectively. For transitions between excited levels with $n > 2$, agreement was to within $\sim 20\%$ for most transitions.

These results were deemed satisfactory for continuation within the collision calculation. In addition to the 31 levels listed in table 1, our $n = 5$ calculation for Fe^{24+} also included the 18 levels arising from the $1s5l$, $l = 0$–4, configurations, giving rise to a 49-level R-matrix calculation. It was verified that regeneration of the energy levels within the R-matrix calculations was accurate to within 10^{-7} Ryd and, as such, no re-ordering took place.

2.3. Collisional calculation details

The inner-region solutions were obtained using R-matrix codes which are based upon the published exchange codes of Berrington *et al* (1995) and the non-exchange codes of Burke *et al* (1992). The outer-region solutions were obtained in an LS-coupling scheme using the code STGFDAMP and the intermediate coupling frame transformation was applied using the code STGICFDAMP. At high angular momenta and/or energies, no resonances are resolved and/or present and it is more efficient to use the undamped versions of these codes, namely STGF and STGICF.

We used 40 continuum basis orbitals per angular momentum within the exchange R-matrix codes. The non-exchange R-matrix codes reduce this number progressively as the continuum orbital angular momentum increases. Accurate collision strengths can be generated for electron energies up to about half of the smallest maximum basis-orbital energy. This corresponds to $\approx$1000 Ryd in the case of Ar^{16+} and $\approx$1500 Ryd in the case of Fe^{24+} ($n = 4$ calculation). In the case of the (Fe^{24+}) $n = 5$ calculation, in principle, one should increase the number of basis orbitals or reduce the maximum scattering energy. We chose to use 40 basis orbitals still. This leads to a smallest maximum basis-orbital energy of $\approx$1500 Ryd (at $l = 5$). However, we still computed collision strengths up to 1500 Ryd. Past experience tells us that a severe deterioration in accuracy does not occur until after 1500 Ryd. The maximum basis orbital energy is significantly larger than this for most angular momenta. The results for the forbidden transitions are most sensitive to such an approach as they are dominated by contributions from low angular momenta. We can assess the accuracy of this approach by comparing our effective collision strengths with those determined via our $n = 4$ calculation.

The exchange calculation was performed up to $J = 10.5$ and the non-exchange calculation up to $J = 58.5$. After that, 'top-up' was used to complete the partial collision strength sum over higher values of J. The top-up for non-dipole transitions was calculated by assuming a geometric series in energy, but taking care to switch-over smoothly to the degenerate-energy limiting case (Burgess *et al* 1970). The top-up for dipole transitions was computed using the Burgess (1974) sum rule—a discussion of the stability of this method, and our implementation of it, is discussed by Badnell and Griffin (2001).

We took care to resolve the resonance regions. In the cases of both Ar^{16+} and Fe^{24+}, we used an energy mesh of $1 \times 10^{-5} z^2$ Ryd (z being the ionic charge) wherever resonances were present and a mesh of $1 \times 10^{-3} z^2$ Ryd in regions where resonances were not present. This resulted in a total of $\sim$10 000 energies for each calculation. This energy mesh resolves the primary resonance structure in the detail necessary for the application to the analysis of plasmas. We note that the incorporation of radiation damping at the heart of our approach both reduces and broadens the resonances that we need to resolve. Hence, our effective resolution is greater than that of an, initially, undamped calculation that uses an equivalent energy mesh, as is done in the resonance-fitting approach to the damping of low-n resonances (Sakimoto *et al* 1990).

2.4. Results illustrating key issues

Our $n = 5$ calculation for Fe^{24+} yields effective collision strengths for 1176 transitions and so only illustrative results are presented here. The full set of results, for both Ar^{16+} and Fe^{24+}, for energy levels, dipole radiative rates, infinite-energy Born collision strengths and Maxwell-averaged effective collision strengths has been compiled according to the requirements of the Atomic Data and Analysis Structure (ADAS) Project (data format *adf04*) (Summers 1994,

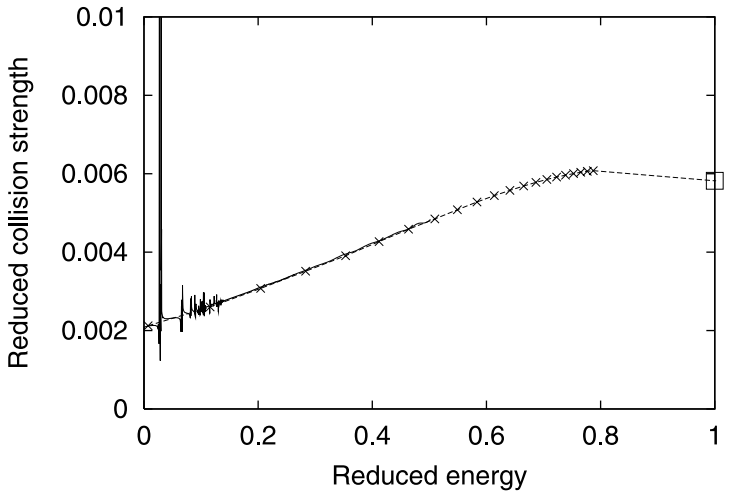

Figure 1. Reduced electron-impact excitation collision strengths for the $1s^2\ ^1S_0$–$1s2p\ ^1P_1$ transition in Fe^{24+} obtained using a reduced-energy parameter of $C = 2$ (see text for details). The full curve denotes the present results and shows the detailed resonance structure. The broken curve and crosses denote the distorted-wave results of Mann (1983). The straight line between the last point of Mann and the infinite-energy limit point (square box) shows the approach to the limit point.

1999) and is available via the world wide web[3]. The tabulated temperature range is 3×10^5–3×10^8 K for Ar^{16+} and 10^6–10^9 K for Fe^{24+}.

Of interest is the quality of data at medium-to-high energies and particular care was taken to check that our results were consistent with the expected infinite-energy limits. We use the 'C-plot' method of Burgess and Tully (1992) to plot a reduced collision strength (Ω_r) against reduced energy (E_r). Here, $\Omega_r(E_r) = \Omega(E_j)/\ln(E_j/E_{ij} + e)$, for a dipole transition, where E_j is the scattered energy and E_{ij} is the excitation energy, for a transition $i \rightarrow j$. The reduced energy is given by $E_r = 1 - \ln(C)/\ln(E_j/E_{ij} + C)$. An example of this is given in figure 1 for the $1s^2\ ^1S_0$–$1s2p\ ^1P_1$ transition in Fe^{24+}. This demonstrates the approach of the reduced collision strength to the infinite-energy limit point (at $E_r = 1$), given by $\Omega_r(1) = 4S/3$, where S is the line strength. Also shown are the results of Mann (1983) which substantiate this paper closely in the high-energy region and clarify the approach to the infinite-energy limit point.

For non-dipole allowed transitions, we make use the infinite-energy Born limit (Burgess *et al* 1997). We have implemented its computation within AUTOSTRUCTURE quite generally and obtain infinite-energy Born collision strengths for all possible transitions and contributing multipoles (Badnell and Thomas, unpublished[4]). We exclude those transitions for which a non-vanishing dipole line-strength exists. In particular, AUTOSTRUCTURE is not restricted to those transitions which contain a contribution from the quadrupole moment, as is the case of SUPERSTRUCTURE (Eissner, private communication). In figure 2, we show the collision strength ($\Omega_r = \Omega$) versus reduced energy (E_r) for the $1s2s\ ^{1,3}S_{0,1}$–$1s4f\ ^3F_3$ transitions in Fe^{24+}. (Now, $E_r = (E_j/E_{ij})/(E_j/E_{ij} + C)$.) Again, we note the approach of the collision strengths to the infinite-energy limit points at $E_r = 1$. It should be noted that the $1s2s\ ^1S_0 - 1s4f\ ^3F_3$ transition is forbidden by the LS-coupling selection rules but spin–orbit mixing with the $1s4f\ ^1F_3$ level

[3] Available from the Oak Ridge Controlled Fusion Atomic Data Center, USA, http://www-cfadc.phy.ornl.gov/data_and_codes/, and the National Institute for Fusions Science, Japan, http://dbshino.nifs.ac.jp/.
[4] The program AUTOSTRUCTURE is available from http://amdpp.phys.strath.ac.uk/autos/.

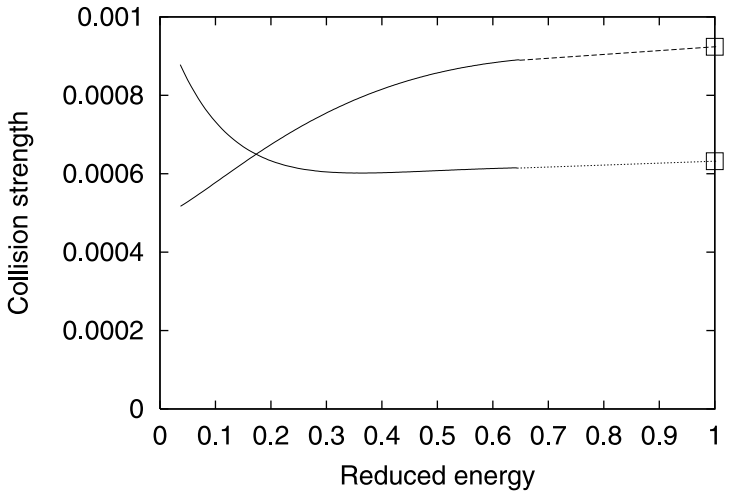

Figure 2. Electron-impact excitation collision strengths for the 1s2s $^{1,3}S_{0,1}$–1s4f $^3F_3$ transitions in Fe^{24+}, obtained using a reduced-energy parameter of $C = 4$ (see text for details). The full curves denote calculated values and the dotted and broken lines link them to their infinite-energy limit points (square boxes), for the 1s2s $^1S_0$ and 1s2s $^3S_1$ initial states, respectively.

gives rise to a non-vanishing Born limit. This type of transition is sometimes described as 'semi-forbidden'. However, from an automated analysis point of view, we classify all transitions with a non-vanishing dipole line strength as dipole, all those with a non-vanishing Born limit as (non-dipole) allowed and all those with a vanishingly small, or zero, limit value as forbidden. The interpolation or extrapolation of the (reduced) collision strengths as a function of (reduced) energy thus follows types 1, 2 and 3 of Burgess and Tully (1992). The issue of a precise definition of 'vanishingly small' only arises for low-charge ions, which is not the case here—this is the Burgess and Tully (1992) type 4 transition.

The effect of radiation damping is also important and an analysis of its effect was performed for both Ar^{16+} and Fe^{24+}. An illustration is shown in figure 3 for the $1s^2\ ^1S_0$–1s3s $^1S_0$ transition. This clearly shows the effect of damping on the lowest-energy resonance group.

3. Application of fundamental data

3.1. Calculation of effective collision strengths

The collision strengths were Maxwell-averaged, using the approach of Burgess *et al* (1997), to generate effective collisions strengths for spectral analysis and modelling. The collision strengths for allowed transitions were interpolated at higher energies using the infinite-energy limit points in the 'C-plot' picture. This gives a more accurate integrand at higher energies and so improves the precision of the effective collision strengths at higher temperatures. In particular, although we only calculated collision strengths up to a scattered (final) energy of ≈ 900 Ryd for Fe^{24+}, we can now tabulate effective collision strengths up to 10^9 K. By looking at the sensitivity to the high-energy interpolation, we estimate the effective collision strengths for the allowed transitions to be accurate to within $\sim$10% at 10^9 K.

The collision strengths for forbidden transitions were extrapolated by assuming an $E^{-\alpha}$ energy dependence, with $\alpha = 1$–2. Formally (Burgess and Tully 1992), an E^{-2} energy dependence is expected, asymptotically. However, some forbidden transitions are enhanced

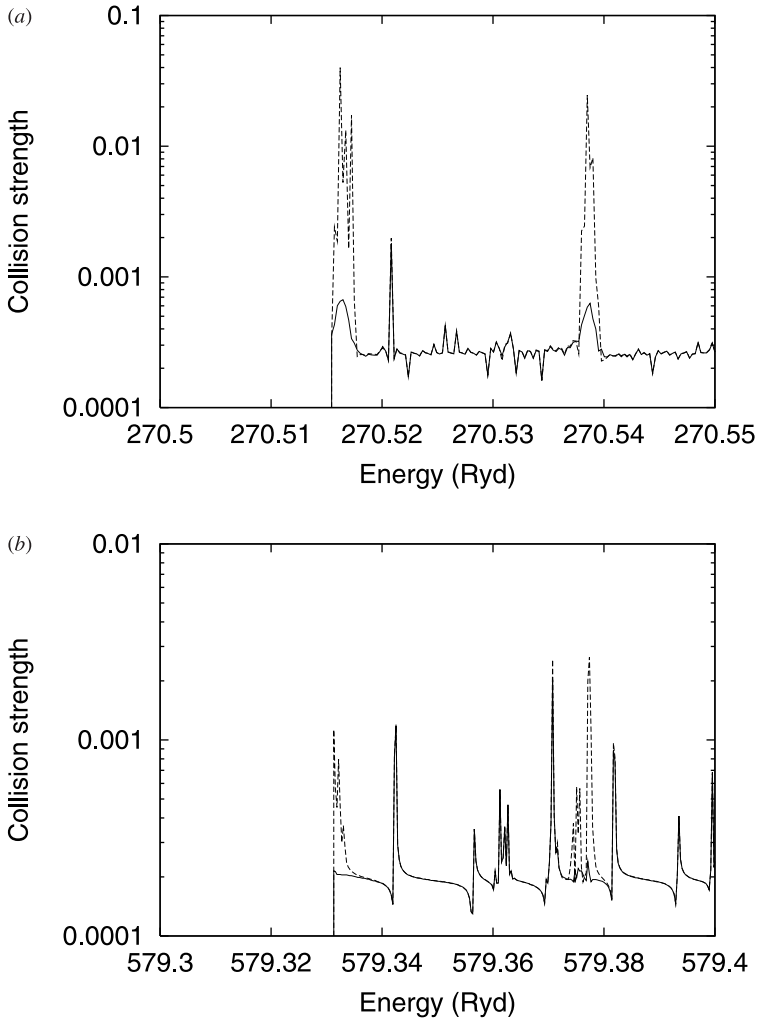

Figure 3. Electron-impact excitation collision strengths for the $1s^2\ {}^1S_0$–$1s3s\ {}^1S_0$ transition in Ar^{16+} (upper) and Fe^{24+} (lower) illustrating a limited energy range of the resonant region near threshold. The full curves denote the damped results and the broken curves denote the undamped results.

by coupling via allowed transitions and so fall-off more slowly with energy, and do not approach their asymptotic limit within our range of calculated energies. The accuracy of the effective collision strengths for forbidden transitions is estimated to be at worst $\sim 20\%$ at 10^9 K. Here, they are even weaker, relatively speaking, than at lower temperatures and are relatively unimportant. Furthermore, the results from our $n = 5$ calculation for Fe^{24+} differ by less than 20% from our $n = 4$ results, at 10^9 K.

Figure 4 illustrates the influence of damping and resonances on the effective collision strength for the $1s2p\ {}^1P_1$–$1s3s\ {}^1S_0$ transition in Ar^{16+}. We see that it is important to allow for both effects at lower temperatures.

We have compared our effective collision strengths with those of Kimura *et al* (2000) for the 16 transitions, out of our 1176, for which they obtained results and we find a broad

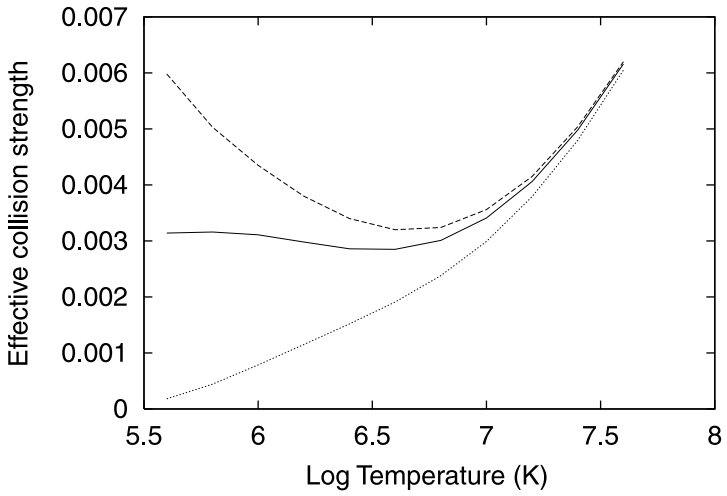

Figure 4. Effective collision strengths for the electron-impact excitation of the 1s2p $^1P_1$–1s3s $^1S_0$ transition in Ar^{16+}. The full curve denotes results that include the radiation damping of resonances. The broken curve denotes results that omit the radiation damping of resonances. The dotted curve denotes results for the underlying (non-resonant) background only.

agreement (to within $\sim 20\%$) for all transitions, at 10^7 K. Two such comparisons are illustrated in figure 5. Very good agreement is found with them for the $1s^2\ ^1S_0$–1s3p $^1P_1$ dipole transition and also with that of Pradhan (1985). The agreement is not so good for the resonance-dominated $1s^2\ ^1S_0$–1s2s $^3S_1$ forbidden transition, although that with Pradhan (1985) is much better. Pradhan (1983b) quoted a 9% reduction of the effective collision strength due to radiation damping for this transition, at a temperature of 2×10^7 K. This is consistent with the results of Kimura *et al* (2000) being higher than ours since they do not allow for radiation damping. There may also be some sensitivity to the resolution of high-n resonances converging on higher $n = 2$ thresholds. We find that the sensitivity to both resonance resolution and to the use of observed versus calculated target level energies gives rise to a less than 2% change in our effective collision strength for this transition at 6.3×10^6 K, which is where the largest disagreement with Kimura *et al* (2000) is to be found. The results of Zhang and Sampson (1987) are somewhat lower than ours and those of Pradhan (1985) in this case.

From the point of view of fundamental excitation data evaluation, it is unlikely that the extension to significantly higher n-shells ($n > 5$) will be undertaken. Yet, for application in low-to-moderate density plasmas, the populations of levels with $n > 5$ deviate from Saha–Boltzmann and must be modelled with explicit reaction rates. Thus, we have given some attention to the problem of the extrapolation of our results to $n > 5$. The broad scaling of the effective collision strengths is as n^{-3}, but we observe deviations from this behaviour. We have used fits to the present data which indicate that errors which are not worse than 30% can be achieved for the extrapolated data. Figure 6 illustrates the result of the extrapolation technique for the 1s2s $^3S_1$–1s5p $^3P_1$ transition in Fe^{24+}. The fitting was performed as $\Upsilon' = an^{-b}$ pointwise on a reduced temperature scale. The latter allows the extrapolation to be extended to the threshold region. The parameters a and b were calculated using the 1s2s $^3S_1$–1s3p $^3P_1$ and 1s2s $^3S_1$–1s4p $^3P_1$ data and then the 1s2s $^3S_1$–1s5p $^3P_1$ data were determined and compared with the explicitly calculated

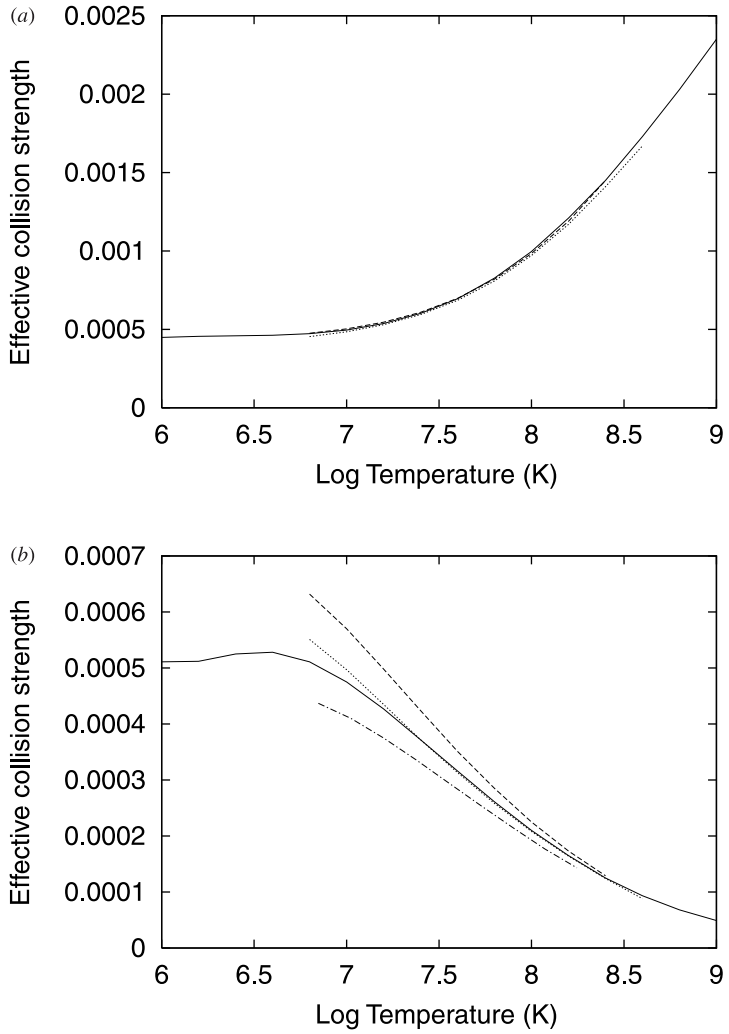

Figure 5. Effective collision strengths for the electron-impact excitation of the $1s^2\ {}^1S_0$–$1s3p\ {}^1P_1$ transition (upper) and the $1s^2\ {}^1S_0$–$1s2s\ {}^3S_1$ transition (lower) in Fe^{24+}. The full curve denotes the present results, the broken curve denotes the results of Kimura *et al* (2000), the dotted curve denotes the results of Pradhan (1985) and the chained curve denotes the results of Zhang and Sampson (1987), lower only.

effective collision strengths. It should be noted that explicit calculations were performed for all transitions up to $n = 5$ and this extrapolation and comparison is merely to investigate the importance of calculating rates explicitly instead of attempting to obtain them via extrapolation.

3.2. Calculation of important line ratios

For application, the present resultant rate-coefficients must be incorporated into excited-population models. We used the Atomic Data and Analysis Structure (ADAS) for our analysis (Summers 1994, 1999).

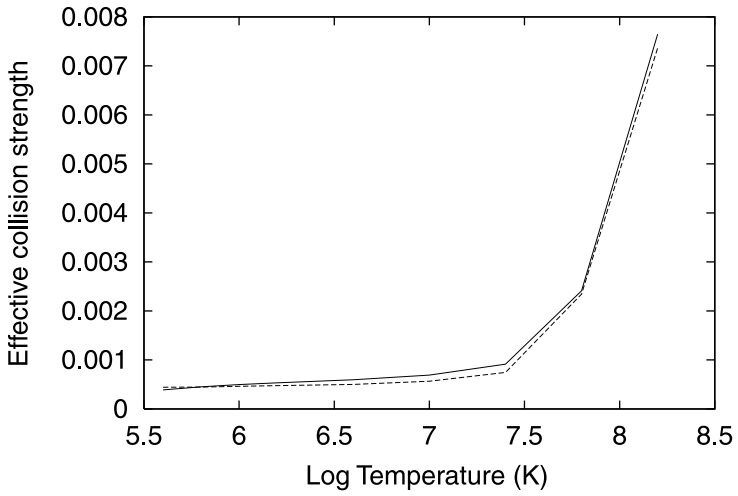

Figure 6. Effective collision strengths for the electron-impact excitation of the 1s2s $^3S_1$–1s5p $^3P_1$ transition in Fe^{24+}. The full curve denotes the explicitly calculated results and the broken curve denotes the results extrapolated from lower n-shells.

We are concerned with the impact of both absolute values of the collision data and its uncertainties on populations and consequential line emission—particularly on the familiar diagnostic line ratios. There are two sources of uncertainty associated with our collision data, namely, the absolute accuracy of rate coefficient evaluation in the R-matrix approach and the uncertainty introduced by our extrapolation procedures for higher quantum-shell rates. It is appropriate also to assess the actual contribution of excitation to higher quantum shells to the populating of lower (especially $n = 2$) levels by cascading and, hence, the contribution to diagnostic line ratios. For this assessment, we adopt a collisional–radiative model that is restricted to levels up to some quantum shell, n_0. All electron-impact collisional and radiative processes are included between these levels, but all other processes, including recombination, are excluded. Thus, it is strictly the excitation driven part of the population structure which is examined.

The completeness of the R-matrix calculations performed here suggests that the absolute error of the rate coefficients should approach the limiting accuracy of the method. We take this to be 10%, as representative of the dominant transitions, for every explicit (non-extrapolated in n) rate coefficient, at all temperatures, and 30% for extrapolated rate coefficients. Also, it is assumed that the error in each rate coefficient can be treated as independent from each other and with a Gaussian distribution of half-width equal to the absolute error. On this basis, a statistical error on each population was computed by Monte Carlo random sampling of the errors in every rate coefficient using the code ADAS216 (Summers 1999). After sufficient samples, the set of results for each population delimits a Gaussian whose half-width is the statistical error in the population, for a given temperature and density.

We found that the error that was propagated to the populations was less than 10%. Table 2 shows the statistical uncertainties for the excited-level populations which give rise directly to the x/y-ratio and the G-ratio ((x + y + z)/w), at a representative temperature and density for both ions. The results isolate the effects of including higher n-shells, using both exact and extrapolated data, with their associated errors. We are able to resolve the contribution from any given rate coefficient to the population of any level. This shows that the uncertainty of the

Table 2. Propagated uncertainty in the populations of the levels responsible for the transitions leading to the x/y-ratio and G-ratio at an electron temperature of 1.58×10^7 K and density of 10^{13} cm^{-3} (Ar^{16+}) and an electron temperature of 3.98×10^7 K and density of 10^{14} cm^{-3} (Fe^{24+}, for several models—see text).

			Fe^{24+}		
Level	Line	Ar^{16+}	$n = 4$	$n = 5$	$n = 5$[a]
1s2p $^1P_1$	w	9.7%	8.3%	8.2%	9.7%
1s2p $^3P_1$	x	4.3%	8.2%	8.1%	9.8%
1s2p $^3P_2$	y	4.7%	9.4%	9.8%	9.3%
1s2s $^3S_1$	z	4.9%	5.1%	5.1%	8.1%

[a] Extrapolated.

1s2s $^3S_1$ population is most affected by the larger uncertainties in the higher-level fundamental rates (see table 2). Note that the 1s2s $^3S_1$ level is long-lived and has a weak direct excitation, thus, cascade from the higher levels is more influential.

4. Conclusions

We conclude that the present effective collision strength data are the most complete in terms of transitions, the inclusion of radiation damping, resolved resonance structure and utilization of infinite-energy limit points. The consideration of the influence of the collisional data upon excited populations removes an uncertainty in modelling the spectral emission of helium-like ions. The methods presented here for creating and verifying collision data will serve as a benchmark for future intermediate coupling frame transformation R-matrix calculations and their application to medium-to-heavy atomic mass helium-like ions.

Acknowledgments

We would like to thank Werner Eissner for providing us with a version of the SUPERSTRUCTURE code with his implementation of the infinite-energy Born limit. This work was supported, in part, by a PPARC Grant (PPA/G/S/1997/00783) with the University of Strathclyde. One of us (ADW) acknowledges a scholarship provided by the Caledonian Research Foundation.

References

Badnell N R 1997 *J. Phys. B: At. Mol. Opt. Phys.* **30** 1–11
Badnell N R and Griffin D C 2001 *J. Phys. B: At. Mol. Opt. Phys.* **34** 681–97
Berrington K A, Eissner W B and Norrington P H 1995 *Comput. Phys. Commun.* **92** 290–420
Bhatia A K and Temkin A 1977 *J. Phys. B: At. Mol. Phys.* **10** 2893–912
Burgess A 1974 *J. Phys. B: At. Mol. Phys.* **7** L364–7
Burgess A, Chidichimo M C and Tully J A 1997 *J. Phys. B: At. Mol. Opt. Phys.* **30** 33–57
Burgess A, Hummer D G and Tully J A 1970 *Phil. Trans. R. Soc.* A **266** 225–79
Burgess A and Tully J A 1992 *Astron. Astrophys.* **254** 436–53
Burke P G and Berrington K A 1993 *Atomic and Molecular Processes—an R-Matrix Approach* (Bristol: IOP Publishing)
Burke V M, Burke P G and Scott N S 1992 *Comput. Phys. Commun.* **69** 76–98
Chantrenne S, Beiersdorfer P, Cauble R and Schneider M B 1992 *Phys. Rev. Lett.* **69** 265–8
Drake G W 1988 *Can. J. Phys.* **66** 586–611
Gabriel A H 1972 *Mon. Not. R. Astron. Soc.* **160** 99–119

Gorczyca T W and Badnell N R 1996 *J. Phys. B: At. Mol. Opt. Phys.* **29** L283–90
——2000 *J. Phys. B: At. Mol. Opt. Phys.* **33** 2511–23
Gorczyca T W, Robicheaux F, Pindzola M S and Badnell N R 1995 *Phys. Rev.* A **52** 3852–9
Griffin D C, Badnell N R and Pindzola M S 1998 *J. Phys. B: At. Mol. Opt. Phys.* **31** 3713–27
Jones M 1974 *Mon. Not. R. Astron. Soc.* **169** 211–27
Kimura E, Nakazaki S, Berrington K A and Norrington P H 2000 *J. Phys. B: At. Mol. Opt. Phys.* **33** 3449–66
Mann J B 1983 *At. Data Nucl. Data Tables* **29** 407–32
NIST 2001 *Atomic Spectra Database* webpage http://physics.nist.gov/
Plante D R, Johnson W R and Sapirstein J 1994 *Phys. Rev.* A **49** 3519–30
Pradhan A K 1983a *Phys. Rev.* A **28** 2113–27
——1983b *Phys. Rev.* A **28** 2128–36
——1985 *Astrophys. J. Suppl.* **59** 183–95
Robicheaux F, Gorczyca T W, Pindzola M S and Badnell N R 1995 *Phys. Rev.* A **52** 1319–33
Sakimoto K, Terao M and Berrington K A 1990 *Phys. Rev.* A **42** 291–5
Sampson D H, Goett S J and Clark R E H 1983 *At. Data Nucl. Data Tables* **29** 467–534
Summers H P 1994 *JET Joint Undertaking Report* JET-IR(94)06
——1999 *ADAS User Manual Version 2.1* webpage http://adas.phys.strath.ac.uk/
Tayal S S and Kingston A E 1984 *J. Phys. B: At. Mol. Phys.* **17** 1383–90
——1985 *J. Phys. B: At. Mol. Phys.* **18** 2983–91
Van Regemorter H 1962 *Astrophys. J.* **136** 906–15
Wong K L, Beiersdorfer P, Reed K J and Vogel D A 1995 *Phys. Rev.* A **51** 1214–20
Zhang H L and Pradhan A K 1995 *J. Phys. B: At. Mol. Opt. Phys.* **28** L285–92
Zhang H L and Sampson D H 1987 *Astrophys. J. Suppl.* **63** 487–514